

# Smooth double barriers in quantum mechanics

Avik Dutt\*

*Department of Electronics and Electrical Communication Engineering,  
Indian Institute of Technology, Kharagpur, 721302, India*

Sayan Kar<sup>†</sup>

*Department of Physics and Meteorology and Center for Theoretical Studies,  
Indian Institute of Technology, Kharagpur, 721302, India*

arXiv:1008.1640v3 [quant-ph] 24 Oct 2021

## Abstract

Quantum mechanical tunneling across smooth double barrier potentials modeled using Gaussian functions, is analyzed numerically and by using the WKB approximation. The transmission probability, resonances as a function of incident particle energy, and their dependence on the barrier parameters are obtained for various cases. We also discuss the tunneling time, for which we obtain generalizations of the known results for rectangular barriers.

## I. INTRODUCTION

The usual example of quantum mechanical tunneling is the rectangular barrier in one dimension.<sup>1-3</sup> Curious students might wonder what happens if we consider smooth barriers. Do the tunneling results remain the same? Are there quantitative or qualitative differences? Students might also wonder what happens if there is more than one barrier. To answer these questions (particularly for smooth barriers), numerical methods and approximations are essential because little can be done analytically. In this paper we discuss tunneling across smooth double barriers of various types.

Double barrier potentials arise in many diverse areas. We give a few examples in the following.

*Quantum heterostructures.*<sup>4,5</sup> Semiconductor heterostructures are layered, thin (about 100 nanometers or less) sandwich structures made with different semiconductor materials (for example, GaAs between two AlAs layers). The existence of junctions of different materials is the reason for the occurrence of sequences of wells and barriers in such structures. Semiconductor heterostructures have made it possible to control the parameters inside crystals and devices such as band gaps and the effective masses of charge carriers and their mobilities, refractive indices, and electron energy spectrum. Heterostructure electronics are widely used in many areas, including laser-based telecommunication systems, light-emitting diodes, bipolar transistors, and low-noise high-electron-mobility transistors for high-frequency applications including satellite television.<sup>5</sup>

*High energy physics.* A barrier penetration model has been developed for heavy ion

---

\* quantumavik@gmail.com

† sayan@iitkgp.ac.in

fusion,<sup>6</sup> taking into account the realistic features of the Coulomb potential for the case of nuclei. The typical barrier shapes encountered for nuclei conform to double barriers.

*Extra dimensions.* Another area where such potentials arise is in the physics of extra dimensions. In particular, they appear in the context of localization of particles and fields on a four-dimensional hypersurface, known as the brane. In these brane-world models<sup>7</sup> localized particles in four dimensions are viewed as bound or quasi-bound (resonant) states in a double barrier effective potential spread across the extra dimensional coordinate.

*Nonlinear Schrödinger equation.* The nonlinear Schrödinger equation has been used in investigations of Bose-Einstein condensates to probe macroscopic quantum tunneling<sup>8–10</sup> and gravity surface waves in fluids, among many other applications. The methods we will discuss here may be extended, with minor modifications, to the Gross-Pitaevskii equation, a nonlinear Schrödinger equation arising in the study of many body systems. Above barrier reflection and tunneling in the nonlinear Schrödinger equation is discussed in Ref. [9]. The double Gaussian barrier, as well as the rectangular barrier, has been used as model potentials in studies<sup>8,10</sup> of the nonlinear Schrödinger equation. However, the definition of the tunneling coefficient is ambiguous for weak nonlinearity, because the principle of superposition does not strictly hold.

Apart from the applications we have discussed, we mention some recent pedagogical articles on double barrier tunneling. Numerical solutions for quantum tunneling through rectangular double barrier heterostructures have been explored.<sup>11</sup> Further, a detailed analysis of the propagation of wave packets across double barriers has been performed.<sup>12</sup> Three-dimensional  $s$ -wave tunneling for double barrier potentials has also been investigated.<sup>13</sup>

The paper is organized as follows. In Sec. II we introduce the various types of double barriers that will be discussed. Section III discusses the theory of double barrier tunneling, and the various methods we will use. Numerical and semiclassical analyses of the smooth barriers mentioned in Sec. II are carried out in Sec. IV. In Sec. V we determine the tunneling time across smooth double barriers. Section VI summarizes our results and mentions some possibilities for future studies.

## II. TUNNELING ACROSS DOUBLE BARRIERS

A simple way to model double barrier potentials is to add a term shifted in position to the single barrier potential function, that is,

$$V(x) = V_{\text{single}}(x, V_1, w_1) + V_{\text{single}}(x - a, V_2, w_2), \quad (1)$$

where  $V_{1,2}$  and  $w_{1,2}$  are the height and width of the two barriers. The separation between the barrier heights is  $a$ .

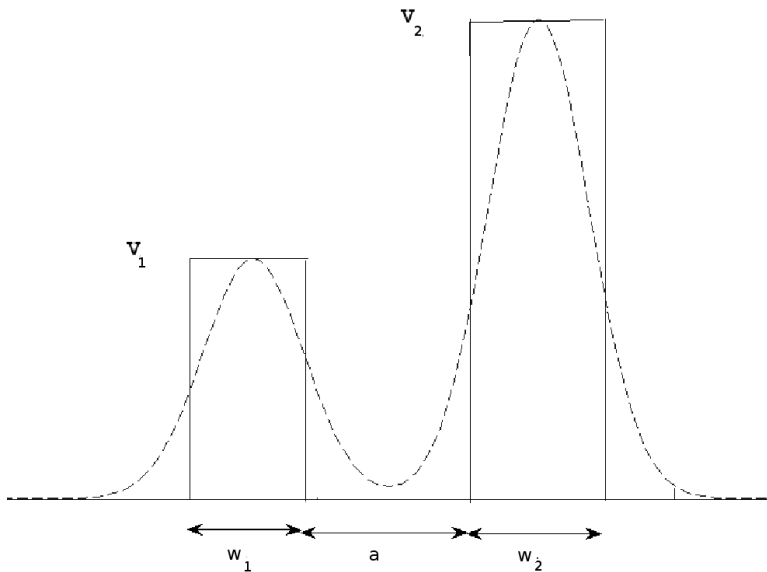


FIG. 1. Rectangular double barrier (solid line) of widths  $w_1$  and  $w_2$  separated by the distance  $a$ . The heights of the two single barrier potentials are  $V_1$  and  $V_2$ . Also shown is a double Gaussian barrier (dashed line).

The simplest and the easiest barrier to analyze is the rectangular double potential barrier, whose parameters are defined in Fig. 1. We have

$$V_{\text{single}}(x, V_1, w_1) = \begin{cases} 0 & x < 0 \\ V_1 & 0 \leq x \leq w_1 \\ 0 & x > w_1 \end{cases} \quad (2)$$

Similarly, the Gaussian double barrier (see Fig. 1) is written using

$$V_{\text{single}}(x, V_1, \sigma_1) = V_1 e^{-x^2/2\sigma_1^2} \quad (3)$$

and hence  $V(x) = V_{\text{single}}(x, V_1, \sigma_1) + V_{\text{single}}(x - a, V_2, \sigma_2)$ .

The time-independent Schrödinger equation for a one-dimensional potential  $V(x)$  is

$$\frac{d^2\psi}{dx^2} + \frac{2m}{\hbar^2}[E - V(x)]\psi = 0, \quad (4)$$

where  $m$  is the mass of the particle,  $E$  is its energy, and  $\psi$  is the wavefunction. The Schrödinger equation for a rectangular double barrier can be readily solved for  $\psi$ , giving five solutions in the five regions. The solutions and their derivatives can be matched at the boundaries between two regions to obtain a relation between the incoming and outgoing waves. The transmission amplitude is<sup>14</sup>

$$T = 4[e^{ik_1(w_1+w_2)}(2 \cosh(k_3w_2) - ik_{1-3} \sinh(k_3w_2)) \times (2 \cosh(k_2w_1) - ik_{1-2} \sinh(k_2w_1)) + e^{ik_1(g+b-w_1)}k_{1+3}k_{1+2} \sinh(k_2w_1) \sinh(k_3w_2)]^{-1}, \quad (5)$$

where  $w_1$  and  $w_2$  are given in Eq. (1),(2). The other parameters are defined as

$$g = w_1 + w_2, \quad b = w_1 + a + w_2 \quad (6a)$$

$$k_1 = \sqrt{2mE}/\hbar, \quad k_2 = \sqrt{2m(V_1 - E)}/\hbar \quad (6b)$$

$$k_3 = \sqrt{2m(V_2 - E)}/\hbar, \quad k_{i\pm j} = \frac{k_i}{k_j} \pm \frac{k_j}{k_i}, \quad (i, j = 1, 2, 3). \quad (6c)$$

The transmission coefficient (probability) is  $\mathcal{T} = T^*T$ .

For the rectangular double barrier, for which we have analytical solutions, we match  $\psi$  and  $d\psi/dx$  at the discontinuities to obtain the relations between the wavefunction amplitudes, that is,  $A$  and  $C$ . For a smooth barrier, the ratio of  $A$  and  $C$  can be obtained by solving Eq. (4) numerically. The ratio of the maxima on the right-hand side of the barrier to the incident amplitude on the left-hand side of the barrier can be found from the plot of  $\psi$  versus  $x$ .

The analysis can be extended to the arbitrary potential functions.<sup>3,15</sup> However, exact analytical solutions of Eq. (4) are usually difficult or impossible to find. In particular, it is impossible to exactly solve the Schrödinger equation for the Gaussian potential. To obtain useful results, we either find numerical solutions or use the WKB approximation.

To solve the Schrödinger equation numerically, we write Eq. (4) as a system of two first-order linear ordinary differential equations with  $\phi_1 = \psi$  and  $\phi_2 = d\psi/dx$ . With these

substitutions, Eq. (4) becomes

$$\phi_1' = \phi_2, \quad (7a)$$

$$\phi_2' = \frac{2m}{\hbar^2}(V(x) - E)\phi_1. \quad (7b)$$

Equation (7) can be solved for  $\phi_1$  to obtain  $\psi(x)$ . We used the fourth order Runge-Kutta algorithm.

We compute the wavefunction on both sides of the barrier for different energies in the required range (up to twice the maximum potential height of the barriers). Because the potentials are rapidly decaying and we are mainly interested in the barrier penetration properties, the use of asymptotic solutions for  $\psi$  to calculate  $\mathcal{T}$  is justified. To the far right and far left of the well, the forms of  $\psi$  are,

$$\psi_{\text{right}} \rightarrow Ce^{ikx}, \quad \psi_{\text{left}} \rightarrow Ae^{ikx} + Be^{-ikx}. \quad (8)$$

The transmission coefficient is calculated from

$$\mathcal{T} = \frac{|C|^2}{|A|^2}. \quad (9)$$

The Wentzel-Kramers-Brillouin (WKB) approximation<sup>2,16</sup> can be used to obtain partially analytic results for an arbitrary potential well. In this approximation the wavefunction  $\psi$  is expressed as a power series in  $\hbar$ . We write the wavefunction in the form

$$\psi = A(x)e^{i\phi(x)}. \quad (10)$$

If we assume the potential is slowly varying and neglect the second derivatives of  $\phi$  and  $A$ , the solutions of the Schrödinger equation can be expressed as

$$\psi = \tilde{A}|p|^{-1/2}e^{\pm i \int |p| dx/\hbar}, \quad p = \sqrt{2m[E - V(x)]}. \quad (11)$$

The limits of integration in Eq. (11) are determined by the classical turning points at which  $E = V(x)$ . At these points the semiclassical approximation fails because the wavefunction becomes infinite. To the far left and to the far right of the barriers, the WKB method gives reasonably good approximations for  $\psi(x)$ . The matching of  $\psi$  near the classical turning points is done by the use of special functions. The asymptotic forms of these functions result in a net phase shift of  $\pi/4$  when going from a classically forbidden region to a classically allowed region or vice-versa.<sup>2,16</sup>

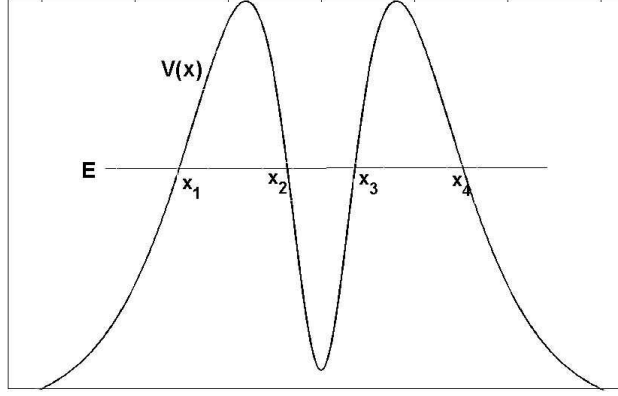


FIG. 2. An arbitrary double barrier potential  $V(x)$  with classical turning points at  $x_1$ ,  $x_2$ ,  $x_3$ , and  $x_4$ . The regions  $x_1 < x < x_2$  and  $x_3 < x < x_4$  are classically forbidden, but the particle can tunnel through these regions quantum mechanically.

For a general single barrier potential, the transmission probability is<sup>16</sup>

$$\mathcal{T} \approx \left( \frac{1}{T} + \frac{T}{4} \right)^{-2} = T^2 / (1 + T^2/4)^2, \quad (12)$$

where

$$T = \exp \left[ - \int_{x_1}^{x_2} \sqrt{2m(V(x) - E)} dx / \hbar \right], \quad (13)$$

and  $x_1$  and  $x_2$  are the classical turning points. The WKB approximation introduces errors which are consistent with  $T$  being small for the single barrier case. Thus  $\mathcal{T} \simeq T^2$ , or

$$\mathcal{T} \simeq \exp \left[ - \frac{2}{\hbar} \int_{x_1}^{x_2} \sqrt{2m(V(x) - E)} dx \right]. \quad (14)$$

For a double barrier we obtain four classical turning points instead of two as evident from Fig. 2. Starting with the wave function on the far right of the barrier (region V), we have

$$\psi_V = Ap^{-1/2} \exp \left( i \int_{x_4}^x p/\hbar dx + i \frac{\pi}{4} \right). \quad (15)$$

Let  $T_1$ ,  $T_2$ , and  $T_3$  be defined as

$$T_1 = \exp \left( - \int_{x_3}^{x_4} |p|/\hbar dx \right) \quad (16a)$$

$$T_2 = \int_{x_2}^{x_3} p/\hbar dx \quad (16b)$$

$$T_3 = \exp \left( - \int_{x_1}^{x_2} |p|/\hbar dx \right) \quad (16c)$$

We expand the complex exponentials using Euler's identity, and then match the real and imaginary parts of  $\psi$  near  $x < x_4$  and  $x > x_4$ , and then near  $x < x_3$  and  $x > x_3$  (by applying the connecting formulae of the WKB method) and obtain

$$\begin{aligned} \psi_{\text{III}} = iAp^{-1/2} & \left[ \left( \frac{T_1}{4} - \frac{1}{T_1} \right) \exp \left( i \int_x^{x_3} p/\hbar dx + \frac{i\pi}{4} \right) \right. \\ & \left. + \left( \frac{T_1}{4} + \frac{1}{T_1} \right) \exp \left( -i \int_x^{x_3} p/\hbar dx - \frac{i\pi}{4} \right) \right]. \end{aligned} \quad (17)$$

Similarly, we find

$$\begin{aligned} \psi_I = \frac{A}{\sqrt{|p|}} & \left[ \left( \frac{C_3 + C_4}{iT_3} + \frac{iT_3C_4 - iT_3C_3}{4} \right) \exp \left( i \int_x^{x_1} p/\hbar dx + \frac{i\pi}{4} \right) \right. \\ & \left. + \left( -\frac{C_3 + C_4}{iT_3} + \frac{iT_3C_4 - iT_3C_3}{4} \right) \exp \left( -i \int_x^{x_1} p/\hbar dx - \frac{i\pi}{4} \right) \right]. \end{aligned} \quad (18)$$

The second term can be identified with the wave incident from the left, and yields the transmission coefficient

$$\mathcal{T} \approx \left| \frac{\psi_V}{\psi_{\text{incident}}} \right|^2 = \left| \frac{T_3(C_4 - C_3)}{4} + \frac{C_3 + C_4}{T_3} \right|^{-2} \quad (19)$$

where

$$C_3 = (1/T_1 - T_1/4) \exp(iT_2) \quad (20a)$$

$$C_4 = (T_1/4 + 1/T_1) \exp(-iT_2) \quad (20b)$$

and  $p(x) = \sqrt{2m[E - V(x)]}$ .

Equation (19) can be applied to a Gaussian double barrier with the assumptions that  $E < V_1, V_2$ ,  $a \gg \sigma_1, \sigma_2$ , and  $a - 3\sigma_1 - 3\sigma_2 > 0$ . Hence,  $x_{1,2} = \pm\sigma_1\sqrt{2(\log V_1 - \log E)}$ , and  $x_{3,4} = a \pm \sigma_2\sqrt{2(\log V_2 - \log E)}$ . The integrations in the WKB method were performed using Simpson's rule.

### III. NUMERICAL AND SEMICLASSICAL ANALYSIS FOR MODEL SMOOTH BARRIERS

#### A. Numerical Analysis

The  $\mathcal{T}$  versus  $E$  plots in Fig. 3 show the variation of the transmission probability with the energy of an electron incident on a one-dimensional Gaussian double barrier. Figure 3



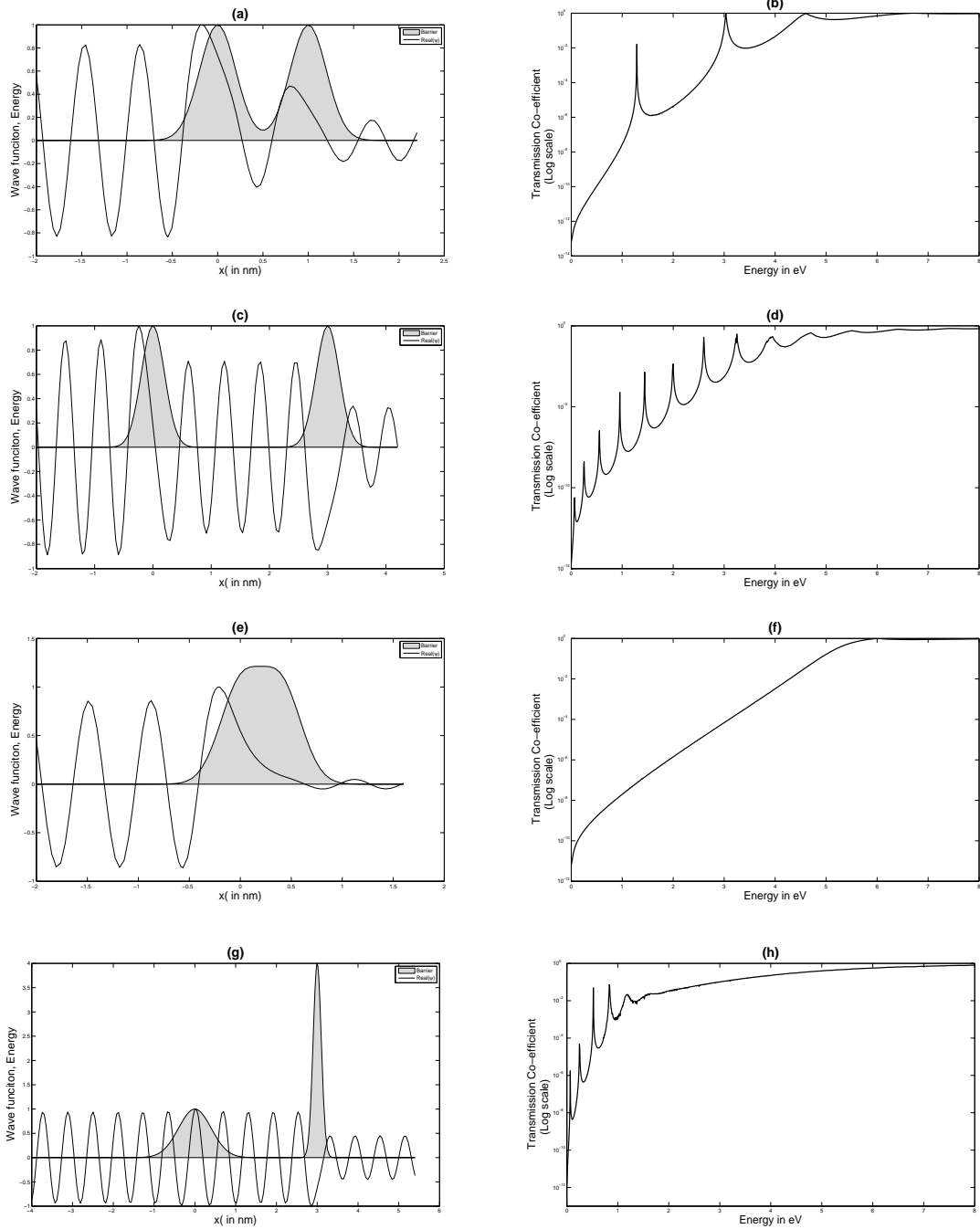


FIG. 3. Plot of the potential (shaded) and wave function. The plots of the wave function are for an incident energy of 4 eV. (a)  $V_1 = V_2 = 4\text{ eV}$ ,  $\sigma_1 = \sigma_2 = 0.2\text{ nm}$ ,  $a = 1\text{ nm}$ . (b) Transmission probability for the barrier in (a). (c)  $V_1 = V_2 = 4\text{ eV}$ ,  $\sigma_1 = \sigma_2 = 0.2\text{ nm}$ ,  $a$  increased to 3 nm. (d) Transmission probability for the barrier in (c) – the number of resonances is greater due to the larger separation-to-width ratio. (e)  $V_1 = V_2 = 4\text{ eV}$ ,  $\sigma_1 = \sigma_2 = 0.2\text{ nm}$ ,  $a$  reduced to 0.4 nm so that the two Gaussian potentials almost merge into a single barrier. (f) Transmission probability for the barrier in (e)– the plot resembles the transmission probability of a single Gaussian barrier. (g)  $V_1 = 1, V_2 = 4\text{ eV}$ ,  $\sigma_1 = 0.4, \sigma_2 = 0.1\text{ nm}$ ,  $a = 3\text{ nm}$ . (h) Transmission probability for the barrier in (g)– asymmetrical barriers have a marked effect on the transmission probability.

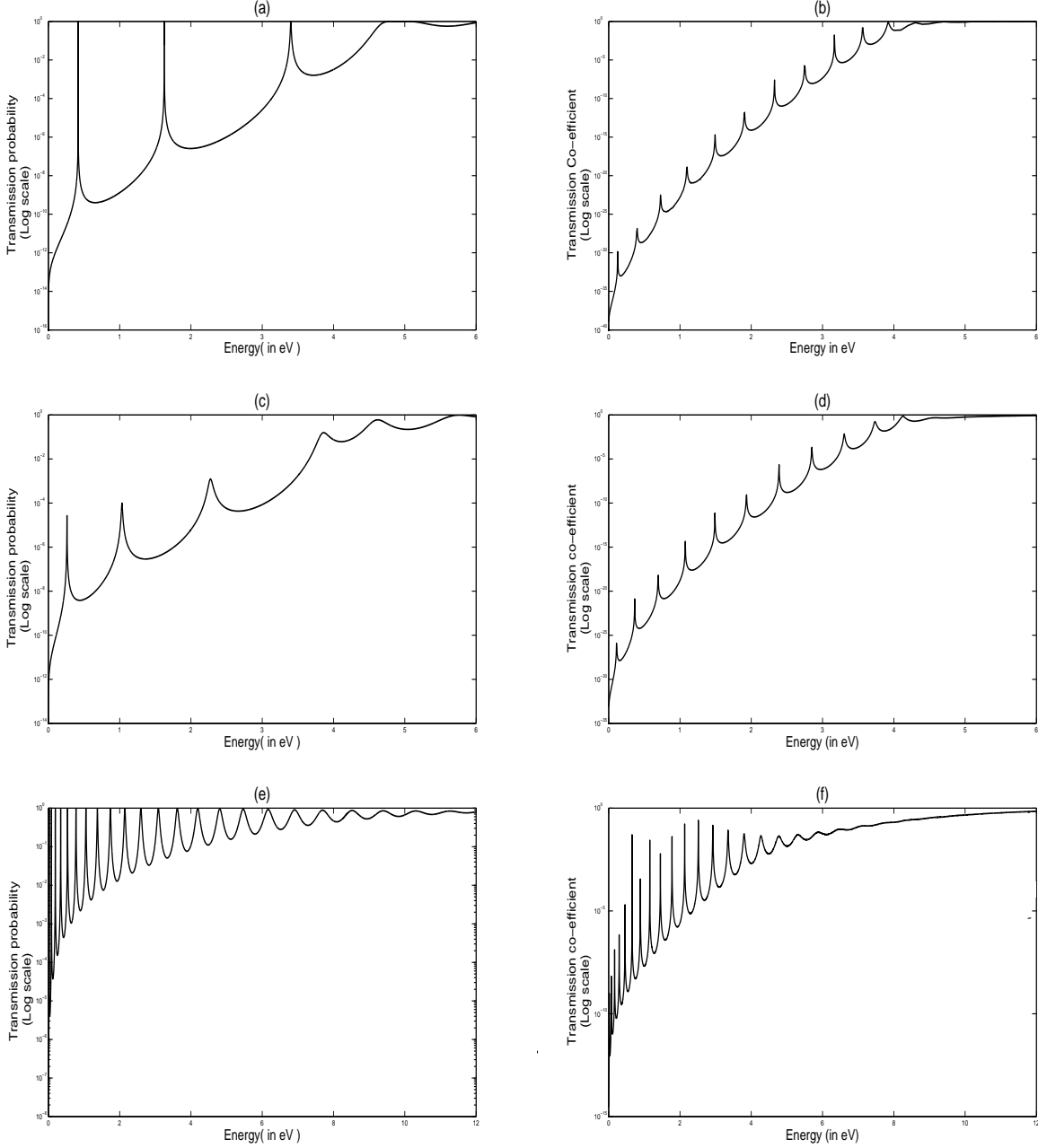


FIG. 4. Comparison of transmission probabilities for the rectangular and the Gaussian double barrier. (a) Square :  $V_1 = 4, V_2 = 4$  eV,  $w_1 = 0.6, w_2 = 0.6, a = 0.75$  nm (b) Gaussian :  $V_1 = 4, V_2 = 4$  eV,  $\sigma_1 = 0.6, \sigma_2 = 0.6, a = 4.35$  nm (c) Square :  $V_1 = 4, V_2 = 4$  eV,  $w_1 = 0.2, w_2 = 0.8, a = 1$  nm (d) Gaussian :  $V_1 = 4, V_2 = 4$  eV,  $\sigma_1 = 0.2, \sigma_2 = 0.8, a = 4$  nm (e) Square :  $V_1 = 4, V_2 = 8$  eV,  $w_1 = 0.2, w_2 = 0.1, a = 4$  nm (f) Gaussian :  $V_1 = 4, V_2 = 8$  eV,  $\sigma_1 = 0.2, \sigma_2 = 0.1, a = 4.9$  nm The transmission probability asymptotically approaches unity for the Gaussian barrier due to the smoothness of the Gaussian barrier potential.

illustrates how the transmission coefficient changes due to the presence of two barriers, a

change in the barrier separation, and a change in the height of one barrier. The energy of the electron is assumed to be of the order of a few electron volts. In Fig. 3(a) the two barriers are very close to each other and the number of resonances is less (Fig. 3(b)) than obtained for larger  $a$ . In Fig. 3(c) the separation between the barriers is increased, the well becomes wider than the well in Fig. 3(a), and consequently, the number of resonances increases (Fig. 3(d)). Figure 3(e) shows two barriers that are so close that they appear to be a single continuous barrier, and hence no resonances (Fig. 3(f)) are seen. In Fig. 3(g) we consider asymmetrical barriers for which  $V_1 \neq V_2$  and/or  $\sigma_1 \neq \sigma_2$  with  $\sigma_1 V_1 = \sigma_2 V_2$ . We note that the effect is predominantly that of a single barrier though resonances do appear (Fig. 3(h)), signaling the presence of a second barrier of much smaller height.

Next, we compare the transmission coefficients for the Gaussian and the rectangular double barrier (see Fig. 4). We choose  $a(\text{Gaussian}) = 3w_1 + 3w_2 + a(\text{rect})$ ,  $\sigma_1 = w_1$ , and  $\sigma_2 = w_2$ . We also vary the height of the barriers keeping the (width  $\times$  height) for both the barriers the same. Figure 4(a),(c),(e) shows the transmission coefficient for a double rectangular barrier, and Fig. 4(b),(d),(f) shows the same for a double Gaussian. The qualitative nature of the plots for the rectangular and the Gaussian barriers is similar. Tunneling occurs for both barriers, though there are differences that may be used to determine the barrier shape from plots of  $\mathcal{T}$  versus  $E$ .

The number of peaks in  $\mathcal{T}$  is large for both cases. However, the peaks and valleys are more prominent for the rectangular barrier. The transmission coefficient for the Gaussian does not reach unity (except asymptotically) and the minima are also at lower values. The cause of this quantitative difference is the smoothness of the Gaussian barrier.

The following observations are valid if  $a/\sigma$  is large ( $\geq 4$ ). The  $\mathcal{T}$  versus  $E$  plot (Fig. 4) depends strongly on the product of width and height for any barrier. If we keep the width  $\times$  height constant, the graphs are qualitatively similar.

The plots show a large number of valleys and peaks, corresponding to resonant states. Resonant states are a result of the destructive interference between waves reflected from the two barriers. The valleys in the  $\mathcal{T}$  versus  $E$  plots correspond to quasi-bound states. As the separation-to-width ratio of the barriers is increased, the number of resonances increases, which means that the well can accommodate a larger number of quasi-bound states. If the well width is made indefinitely wide, the resonant states merge into a continuum.

The peaks become sharper as the height of the barriers is increased; i.e. the full width at

half maximum of the peaks decreases. If  $\Delta$  is the full width at half maximum of the peak in  $\mathcal{T}(E)$ , then  $\Delta$  decreases as  $V_0$  and  $V_1$  increase. The peaks also become sharper if the widths of the barriers are increased, which makes it difficult to obtain numerical solutions. The lower the energy at which the peak occurs, the steeper is the peak. If  $E \ll V_0, V_1$ ,  $\Delta$  is very small and vice versa.

## B. WKB Analysis

The WKB method provides a way of obtaining analytical expressions for the transmission coefficient. In Figure 5 we compare the results obtained for the transmission probability using the semiclassical analysis method and the numerical solutions. Figures 5(a) and (b) differ because of the larger value of  $a$  in Fig. 5(b) (all other parameters are the same). In Fig. 5(c) the heights are halved, and the widths are doubled compared to Fig. 5(b). In Fig. 5(d) the Gaussian barrier is asymmetrical with  $\sigma_1/\sigma_2 = 6$ .

For  $E \ll V_1$  the values of  $\mathcal{T}$  are almost the same, or at least of the same order of magnitude using either the numerical method or the WKB approximation. The greatest deviations from the numerical solution are observed for energies near  $V_0$ . This deviation is expected because the WKB approximation is not valid near the classical turning points. The difference between the WKB method and the numerical solution of Schrodinger's equation also becomes prominent when the separation between the barriers becomes comparable to the width of the barriers. In the calculation of the turning points we neglected the contribution of the first barrier to the turning points of the second barrier and vice versa so that we could obtain analytic expressions for the classical turning points; otherwise, we would have to solve the transcendental equation  $V(x) = [V_1 \exp(-x^2/2\sigma_1^2) + V_2 \exp(-(x-a)^2/2\sigma_2^2)] = E$  for each value of  $E$ . Thus the difference between the semiclassical results and the numerical solutions for the transmission probability becomes prominent when the barriers are close to each other, but the assumption yields acceptable results in return for a shorter computation time.

The WKB approximation becomes more accurate as the separation between the barriers increases. The numerical values of  $\mathcal{T}(E)$  versus  $E$  in Fig. 5 do not match the WKB approximation results for energies  $E > \min(V_1, V_2)$ . For asymmetrical barriers with non-identical potential heights, the WKB approximation breaks down for  $E > \min(V_1, V_2)$  because the

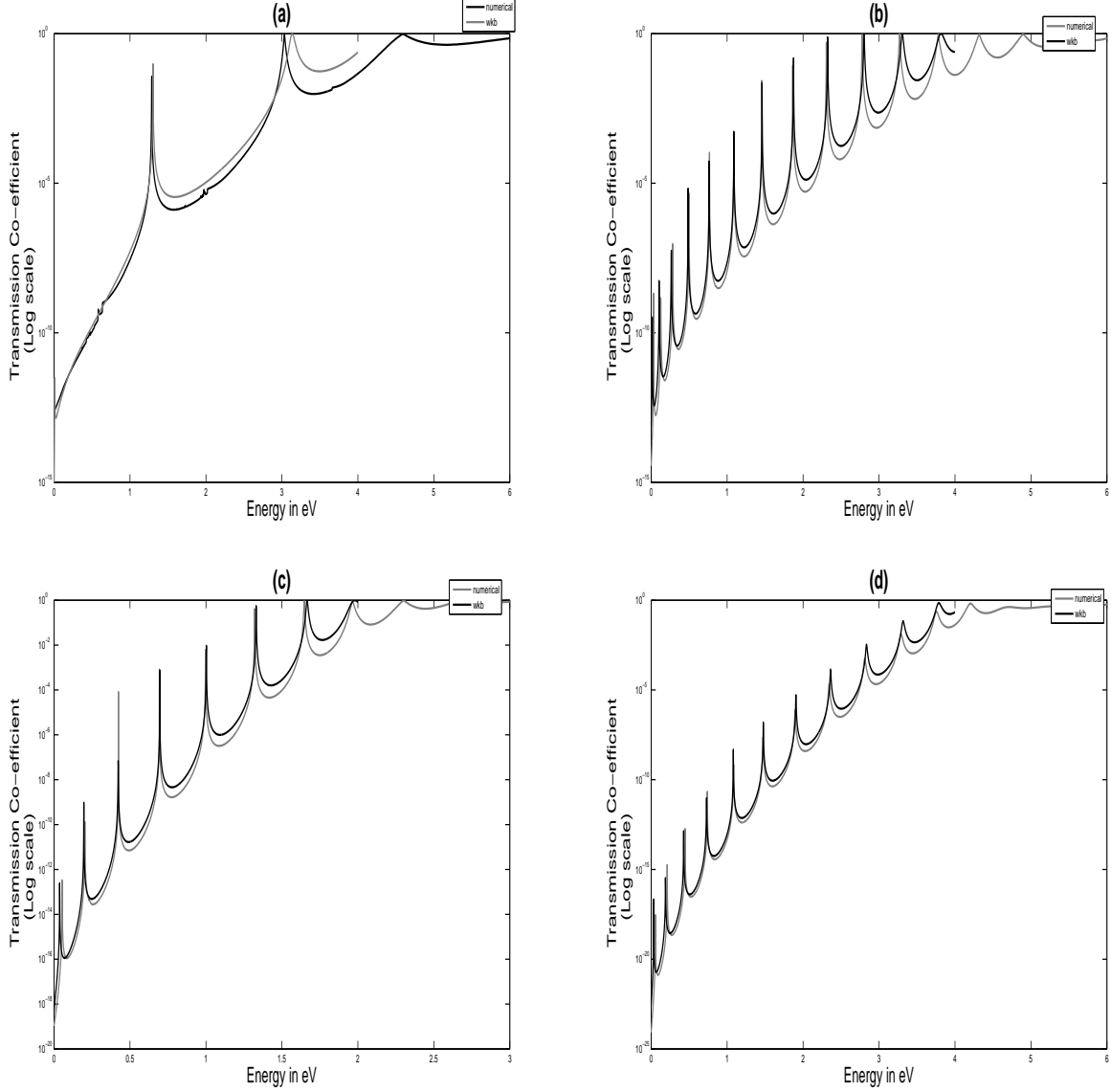


FIG. 5. Comparison of the transmission probabilities calculated by numerical solution of Schrödinger equation (gray) and the WKB approximation (black) for a Gaussian double barrier with parameters: (a)  $V_1 = V_2 = 4 \text{ eV}$ ,  $\sigma_1 = \sigma_2 = 0.2 \text{ nm}$ ,  $a = 1 \text{ nm}$ , (b)  $V_1 = V_2 = 4 \text{ eV}$ ,  $\sigma_1 = \sigma_2 = 0.2 \text{ nm}$ ,  $a$  is increased to  $4 \text{ nm}$ . (c)  $V_1 = V_2 = 2 \text{ eV}$ ,  $\sigma_1 = \sigma_2 = 0.4 \text{ nm}$ ,  $a = 4 \text{ nm}$ . The potential barrier height is larger for this barrier. (d)  $V_1 = V_2 = 4 \text{ eV}$ ,  $\sigma_1 = 0.6$ ,  $\sigma_2 = 0.1 \text{ nm}$ ,  $a = 4 \text{ nm}$ . In this case we consider an asymmetrical barrier. The results obtained by the two methods are in good agreement.

formulation we have used involves four classical turning points. The potential function reduces to a single barrier with two turning points for  $E > \min(V_1, V_2)$ . However, the WKB

results agree quite well for  $E < \min(V_1, V_2)$ .

The advantages of the WKB method are that it requires about an order of magnitude less computation time than the direct numerical solution of Schrodinger's equation. The main limitation of the WKB method is that it relies heavily on the turning points, and hence is difficult to apply to energies greater than the potential height of any of the barriers.

#### IV. TUNNELING TIME

With the advent of the fabrication of nanometer semi-conductor structures, the calculation of tunneling time has acquired more importance.<sup>17</sup> For one-dimensional single barriers, the tunneling time becomes independent of the barrier width for opaque barriers. This ‘‘Hartman effect’’<sup>18</sup> predicts superluminal and arbitrarily large group velocities inside sufficiently long barriers. There is some controversy concerning the definition of the tunneling time.<sup>19</sup> The expression for the tunneling time we have used is variously named the ‘‘group delay’’ or ‘‘phase time.’’

If we assume a single rectangular barrier, with the potential

$$V(x) = \begin{cases} V_0 & (0 < x < L) \\ 0 & \text{elsewhere,} \end{cases} \quad (21)$$

the wavefunction may be written as<sup>19</sup>

$$\psi(x) = \begin{cases} \exp(ikx) + \sqrt{\mathcal{R}} \exp(-ikx + i\gamma) & (x < 0) \\ \psi_1(x) & (0 \leq x \leq L) \\ \sqrt{\mathcal{T}} \exp(ikx + i\alpha) & (x > L). \end{cases} \quad (22)$$

where  $\mathcal{T}$  and  $\mathcal{R}$  are the transmission and reflection probabilities,  $k$  the wave vector, and  $\alpha$  and  $\gamma$  are phase constants dependent on  $k$ . If we apply the stationary phase approximation to the peak of the transmitted wave packet,  $\partial\{\arg(\psi(x, t))\}/\partial k = 0$ , we find

$$\frac{d\alpha}{dk} - \frac{1}{\hbar} \frac{dE}{dk} t = 0. \quad (23)$$

Thus, the temporal delay may be defined as

$$\tau = \hbar \frac{\partial\alpha}{\partial E}. \quad (24)$$

From the transmission amplitude for a single barrier we find the phase shift to be  $\alpha = -\tan^{-1}((\kappa^2 - k^2) \tanh(\kappa L)/2\kappa k)$ , where  $\kappa = \sqrt{2m(V_0 - E)}/\hbar$  and  $k = \sqrt{2mE}/\hbar$ . By using Eq. (24) we have

$$\tau_g \xrightarrow{\kappa L \rightarrow \infty} \frac{2m}{\hbar k \kappa}, \quad (25)$$

where the subscript  $g$  denotes group delay.

For a rectangular double barrier the transmission amplitude is expressed by Eq. (5), and the phase time is<sup>20,21</sup>

$$\tau_g = \hbar \frac{\partial}{\partial E} \arg[T \exp(ik_1 b)]. \quad (26)$$

In the limit of  $k_2 w_1$  and  $k_3 w_2 \rightarrow \infty$ , the phase time becomes independent of the barrier width and separation:

$$\tau_g = \frac{2m}{\hbar k_1 k_2}, \quad (27)$$

except at resonance and anti-resonance.

To illustrate what happens at resonance and anti-resonance,<sup>22</sup> we take  $E = V_1/2$  and  $V_0 = V_1 = V_2$ . When the phase shift  $2k_1 a = 2m\pi$  ( $m = 1, 2, 3, \dots$ ) (resonance), the group delay becomes

$$\tau_g^{\text{res}} = \frac{(1 + R_0) a}{T_0 v}, \quad (28)$$

where  $v = p/m = \sqrt{2mE}/m$ , and  $R_0$  and  $T_0$  denote the reflection and transmission probabilities through a single barrier of width  $w_1$ . At anti-resonance ( $2k_1 a = (2m + 1)\pi$ ),

$$\tau_g^{\text{anti-res}} = \frac{T_0 a}{(1 + R_0) v}, \quad (29)$$

indicating that the phase time increases linearly with the inter-barrier separation,  $a$ , at both resonance and anti-resonance.

### A. Tunneling times for general double barrier potentials

The wave function for  $x > x_4$  (Fig. 2) is given in the WKB approximation by

$$\psi_V = A|p|^{-1/2} \exp\left(\frac{i}{\hbar} \int_{x_4}^x |p| dx + i\frac{\pi}{4}\right), \quad (30)$$

and the incident wavefunction is

$$\psi_{\text{incident}} = A|p|^{-1/2} \{i(C_3 + C_4)/T_3 + iT_3(C_4 - C_3)/4\} \exp\left(-i \int_x^{x_1} p/\hbar dx - i\pi/4\right). \quad (31)$$

In analogy with Eq. (26), the group delay is found to be

$$\tau_g = \hbar \frac{\partial}{\partial E} \arg \left[ (\psi_V / \psi_{\text{incident}}) \exp \left( \int_{x_1}^{x_4} |p| / \hbar dx \right) \right]. \quad (32)$$

If we substitute  $\psi_V$  and  $\psi_{\text{incident}}$ , into Eq. 32 we obtain

$$\tau_g = \hbar \frac{\partial}{\partial E} \arg \left[ \frac{T_3(C_4 - C_3)}{4} + \frac{C_4 + C_3}{T_3} \right]^{-1}, \quad (33)$$

and after some algebra

$$\tau_g = \hbar \frac{\partial}{\partial E} \tan^{-1} \frac{2 \tan T_2}{T_1^2} \quad (34a)$$

$$= \frac{2}{T_1^4 + 4 \tan^2 T_2} T_1^2 \left( \sec^2 T_2 \frac{\partial T_2}{\partial E} - 2 \frac{\tan T_2}{T_1} \frac{\partial T_1}{\partial E} \right). \quad (34b)$$

Equations 27–29, which are applicable for a rectangular barrier, can be recovered from Eq. (34) as follows. We have  $T_1 = \exp(-k_2 w_1)$  and  $T_2 = k_1 a$ . We let  $\phi = \tan^{-1}(2 \tan(T_2)/T_1^2)$  and write  $\tau_g = \hbar \partial \phi / \partial E$ . We find that the phase tunneling time through a rectangular double barrier of width  $w_1$  and separation  $a$  is

$$\tau_g = 2 \cos^2 \phi \frac{m}{\hbar} \exp(2k_2 w_1) (a \sec^2(k_1 a) / k_1 - 2w_1 \tan(k_1 a) / k_2). \quad (35)$$

To illustrate the behavior of  $\tau_g$  near a resonance, we assume  $E = V_1/2$  so that  $k_1 = k_2$ . At resonance,  $2k_1 a = 2m\pi$ , where  $m$  is an integer. The group delay at resonance assumes the form

$$\tau_g^{\text{res}} = 2e^{2k_2 w_1} a / v \approx (1 + R_0) a / T_0 v, \quad (36)$$

because  $\cos \phi = 1$  and  $\tan k_1 a = 0$ . Here,  $R_0 = (1/T_1 - T_1/4)^2 / (1/T_1 + T_1/4)^2$  and  $T_0 = (1/T_1 + T_1/4)^{-2}$  are the reflection and transmission probabilities through a single barrier ( $(1 + R_0)/T_0 = 2(T_1^{-2} + T_1^2/16) \approx 2e^{k_2 w_1}$ ).

Similarly at anti-resonance ( $2k_1 a = (2m + 1)\pi$ ),  $m$  an integer, we have

$$\tau_g^{\text{anti-res}} = T_0 a / v (1 + R_0). \quad (37)$$

We next obtain  $\tau_g$  for a Gaussian double barrier. The relevant integrations for obtaining  $T_3$  are performed numerically. Figure 6 shows the variation of  $\tau_g$  with  $\sigma$  for fixed  $a$ . Figures 7(a) and (b) show how  $\tau_g$  varies with  $a$  for fixed  $\sigma$ .

We see that the group delay increases with an increase in the barrier width up to a certain value and then falls off rapidly on widening the barrier further. The peak in the group delay



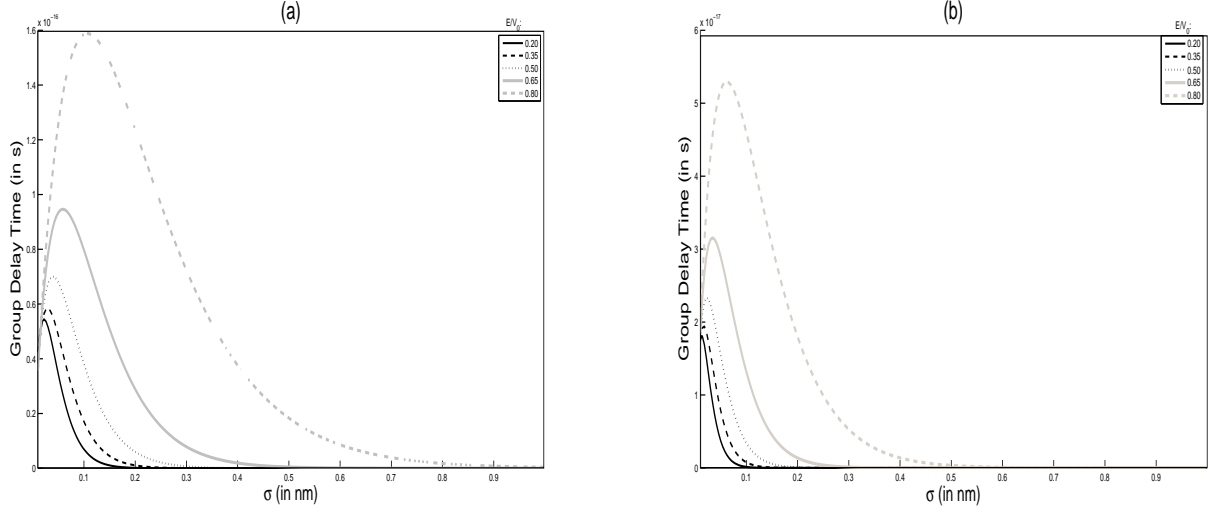


FIG. 6. Variation of tunneling time with barrier width  $\sigma$  for a double Gaussian barrier, with (a)  $V_0 = 4 \text{ eV}$ ;  $a = 8 \text{ nm}$  (b)  $V_0 = 12 \text{ eV}$ ;  $a = 8 \text{ nm}$ , for various energies. The tunneling time increases up to a certain value of  $\sigma$  and then decreases rapidly. The maximum in the curve shifts to larger values of the barrier width for higher energies.

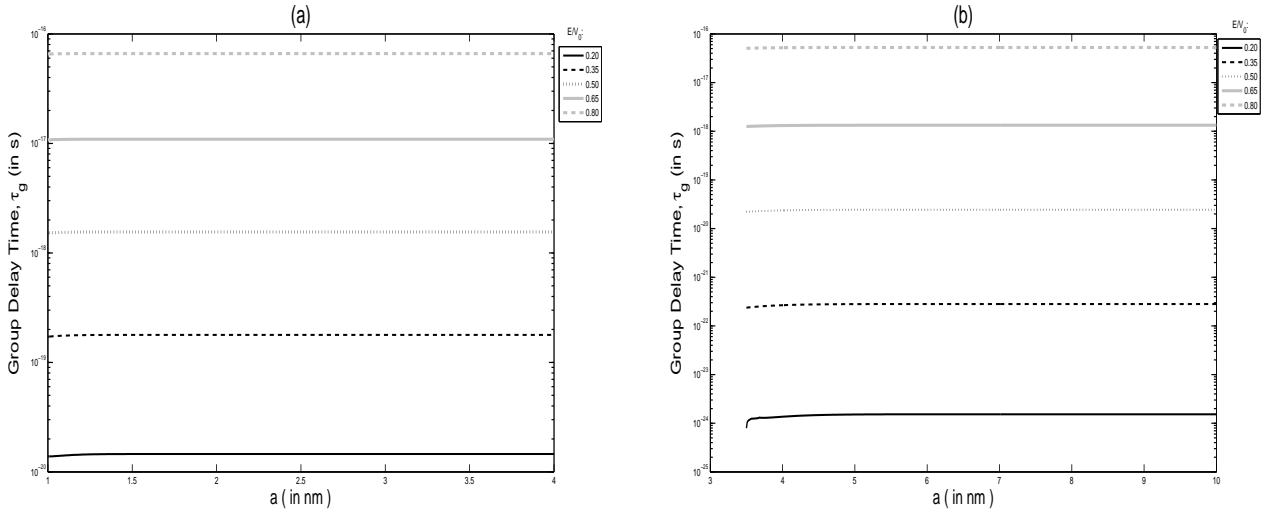


FIG. 7. Variation of the tunneling time through a double Gaussian barrier with inter-barrier distance  $a$  for (a)  $V_0 = 6 \text{ eV}$ ,  $\sigma_1 = 0.2 \text{ nm}$ , and (b)  $V_0 = 1.50 \text{ eV}$ ,  $\sigma_1 = 0.8 \text{ nm}$ . Note that the tunneling time varies over several orders of magnitude, for various energies of the incident particle.

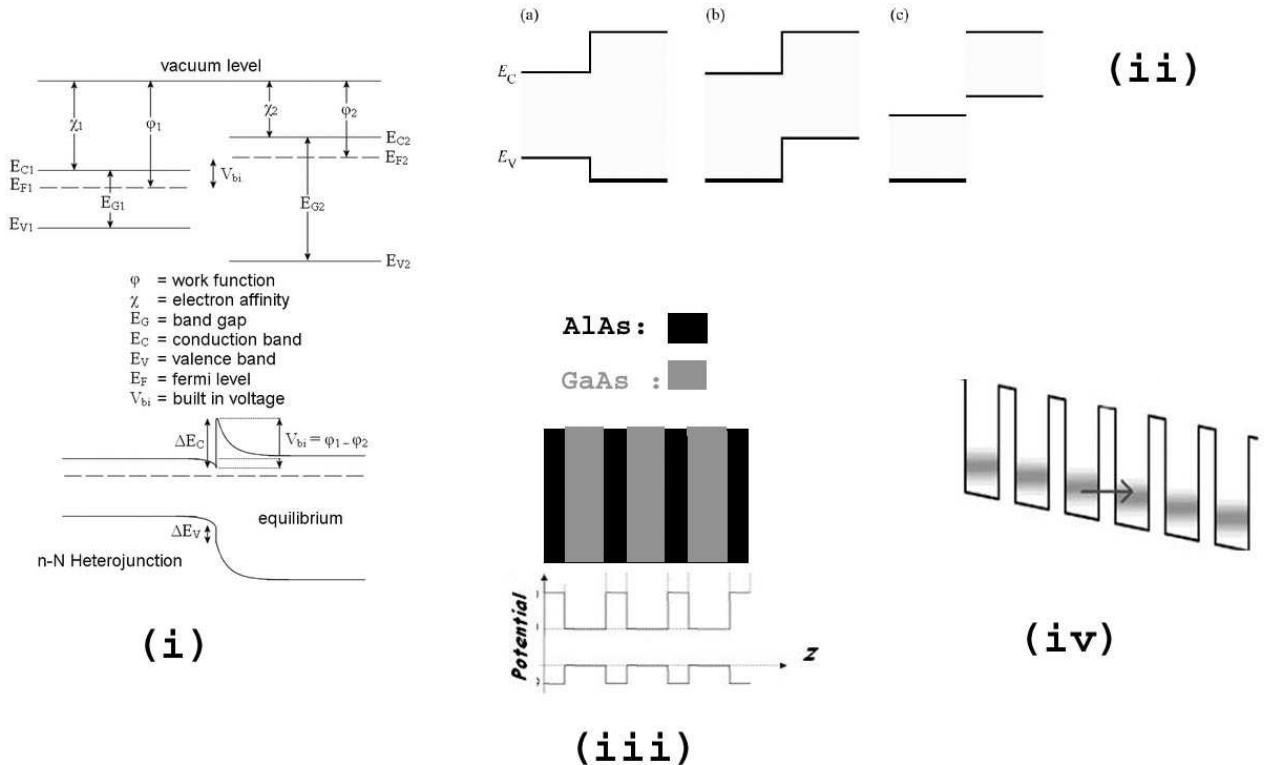
versus barrier width shifts toward the greater widths at higher energies. The maxima in  $\tau_g$  shift to greater values of  $\sigma$  at higher energies. The group delay decreases with increasing

$V_0$ , and for fixed  $V_0$   $\tau_g$  increases with  $E$  if other parameters remain constant. The tunneling time is more or less independent of the interbarrier distance as is evident from Fig. 7, which is consistent with the Hartman effect.

## V. DOUBLE BARRIERS IN HETEROSTRUCTURES

Double barriers of either type (smooth or square) appear in various physical situations (as outlined in Sec. I). We now discuss in some detail, how they may arise in the context of one such scenario-semiconductor heterostructures.

FIG. 8. Semiconductor heterostructures and superlattices: (i) Energy band diagram of an n-N semiconductor heterojunction; (ii) Heterojunctions can be of three types classified according to the lineup of the conduction and valence bands: straddled ( $E_{C2} > E_{C1}, E_{V2} < E_{V1}$ ), staggered ( $E_{C2} > E_{C1}, E_{C1} > E_{V2} > E_{V1}$ ), and broken ( $E_{C2}, E_{V2} > E_{C1}$ ); (iii) An unbiased GaAs/AlGaAs superlattice and the corresponding potential energy diagram; (iv) A biased superlattice created by the application of an electric field, which creates a gradient in the potential function.



A heterojunction (Fig. 8(i),(ii)) is the interface between two dissimilar solid state ma-

materials, including crystalline and amorphous structures of metals, insulators, and semiconductors. A combination of one or more heterojunctions in a device is a heterostructure. As discussed in Sec. I, heterostructures having semiconductor substrates are widely used in the fabrication of devices that have desired electron characteristics as functions of applied potentials.<sup>4</sup>

Quantum structures may be classified as wells, wires, or dots, depending on whether the carriers are confined in one, two or three dimensions. Semiconductors can be used in all of these structures, but we consider one-dimensional potential wells and barriers, which can be fabricated by growing a single layer of one material (such as GaAs) between two layers of different materials (such as AlGaAs), as in Fig. 8(iii). Other pairs of semiconductors having profound importance in technological applications include the III-V compounds GaInAs/InP, GaInAs/AlInAs, GaSb/InSb and the II-VI compounds CdZnSe/ZnSe, ZnSTeSe/ZnSSe.

In a semiconductor the difference between the conduction and valence band energies of the two materials at the heterojunction with respect to the vacuum level and the Fermi level is responsible for the formation of quantum wells, whose heights are of the order of a few hundred meV. This height is to be compared with the thermal energies of carriers at room temperature ( $\approx 26$  meV). Hence, the thermal motion of the electrons does not allow them to frequently cross the barriers, and quantum mechanical tunneling is the main transport phenomena at length scales less than the mean free path of the electrons.

From Fig. 8(i) it is evident that the conduction band potential step is given by  $\Delta E_c = \chi_1 - \chi_2$ . Because the Fermi level must be continuous in chemical and thermal equilibrium, the valence band potential step is found to be  $\Delta E_v = E_{G2} - E_{G1} - \Delta E_c$ .

The I-V characteristics of a one-dimensional quantum heterostructure can be related to the transmission probability according to the relation<sup>23</sup>

$$J = \frac{e}{4\pi^3\hbar} \int_0^\infty dk_l \int_0^\infty dk_t [f(E) - f(E')] T^* T \frac{\partial E}{\partial k}, \quad (38)$$

where  $k_l$  and  $k_t$  are the wave vectors in the longitudinal and transverse directions respectively, and  $f$  is the density of states given by the Fermi-Dirac distribution. The theoretical results can be compared with experimental data available from the current-voltage characteristics of the device. The mass to be used in the Schrödinger equation is the effective mass of the electron  $m^*$  in the longitudinal direction. As mentioned in Ref. [23] the electrons lose coherence after tunneling through a distance of the order of the mean free path of the

carriers, resulting in a widening of the peaks in the I-V characteristics. Calculations of the bound and quasi-bound states of quantum heterostructures are available.<sup>24</sup>

There are two major approximations in the modeling of semiconductor heterostructures by rectangular potentials. The effective mass  $m^*$  of the carrier changes when the electrons pass through a heterojunction, but this variation is not incorporated in the analysis. Also, the potential profile is not steplike – the energy bands of the two materials at the heterojunction change smoothly because of factors such as the inhomogeneities present at the interface, space-dependent composition of the compounds, and possible mechanical strain of the layers. The best known example is the  $\text{SiO}_2/\text{Si}$  heterojunction with a very small density of defects at the interface. Compound semiconductors usually have a larger concentration of defects and inhomogeneities, leading to a continuous barrier rather than a rectangular one.<sup>25,26</sup> The experimental data indicate a double Gaussian distribution of heights for the potential barriers. Another major reason for the smoothening of the heterojunction potential shapes is the formation of a space charge.<sup>27</sup>

Our results may be used to compare models with experimental data which are available for semiconductor heterostructures. This aspect requires more work – we need to find out the theoretical I-V characteristics from the transmission coefficients obtained by using Eq. (38). In principle, other functional forms may also be chosen and the I-V characteristics obtained and compared with experiments to determine the actual distribution of barrier heights. It is possible that such investigations may help design device applications where precise knowledge about fabricated structures is often very useful.

## VI. REMARKS

We have carried out similar computations for the Lorentz barrier, and obtained results closer to the rectangular barrier than to the Gaussian barrier. Other functional forms of the barriers may be studied to learn their characteristic features. A further challenging problem is to consider multiple barriers and external, applied field effects, which are necessary to model realistic systems in condensed matter/semiconductor physics.

## ACKNOWLEDGMENTS

We express our gratitude to the anonymous reviewers for their valuable suggestions in improving the article. We would also like to thank Prof. Sudipta Sarkar and Dr. Kabir Chakravarti for pointing out a misplaced parenthesis in Eq. (5).

- 
- [1] A. Beiser, *Concepts of Modern Physics* (McGraw-Hill International, Singapore, 1984). See Chap. 5 for a discussion on the tunneling effect and Chap. 12 for its application to  $\alpha$ -decay.
  - [2] E. Merzbacher, *Quantum Mechanics* (John Wiley & Sons, New York, 1986).
  - [3] C. Cohen-Tannoudji, B. Liu, and F. Laloe, *Quantum Mechanics*, Vol. 1 (John Wiley & Sons, New York, 1977).
  - [4] V. V. Mitin, V. A. Kochelap, and M. A. Stoscio, *Quantum Heterostructures: Microelectronics and Optoelectronics* (Cambridge University Press, Cambridge, UK, 1999), pp. 73–87.
  - [5] Z. I. Alferov, “The double heterostructure concept and its applications to physics, electronics and technology,” *Rev. Mod. Phys.* **73**(3), 767–782 (2001).
  - [6] P. Descouvemont, D. Baye, and P.-H. Heenen, “A barrier penetration model for heavy ion fusion valid at all energies,” *Z. Phys. A* **306**, 79–88 (1982).
  - [7] L. Randall and R. Sundrum, “An alternative to compactification,” *Phys. Rev. Lett.* **83**, 4690–4693 (1999) *ibid.* “A large mass hierarchy from a small extra dimension,” *Phys. Rev. Lett.* **83**, 3370–3373 (1999).
  - [8] K. Rapedius and H. J. Korsch, “Barrier transmission for the one-dimensional nonlinear Schrodinger equation: Resonances and transmission profiles,” *Phys. Rev. A* **77**, 063610 (2008).
  - [9] H. A. Ishkhanyan and V. P. Krainov, “Above barrier reflection of cold atoms by resonant laser light within the Gross-Pitaevskii approximation,” *Laser Physics* **19**, 1729–1734 (2009); H. A. Ishkhanyan and V. P. Krainov, “Multiple-scale analysis for resonance reflection by a one-dimensional rectangular barrier in the Gross-Pitaevskii problem,” *Phys. Rev. A* **80**, 045601 (2009); H. A. Ishkhanyan, V. P. Krainov, and A. M. Ishkhanyan, “Transmission resonances in above-barrier reflection of ultra-cold atoms by the Rosen-Morse potential,” *J. Phys. B: At. Mol. Opt. Phys.* **43**, 085306 (2010).

- [10] T. Paul, K. Richter, and P. Schlagheck, “Nonlinear resonant transport of Bose-Einstein condensates,” *Phys. Rev. Lett.* **94**, 020404 (2005).
- [11] B. Mendez and F. Dominguez-Adame, “Numerical study of electron tunneling through heterostructures,” *Am. J. Phys.* **62**, 143–147 (1994).
- [12] A. P. Stamp and G. C. McIntosh, “A time-dependent study of resonant tunneling through a double barrier,” *Am. J. Phys.* **64**, 264–276 (1996).
- [13] A. U. Maheswari, P. Prema, S. Mahadevan, and C.S. Shastri, “Quasi-bound states, resonance tunnelling, and tunnelling times generated by twin symmetric barriers,” *Pramana J. Phys.* **73**(6), 969–988 (2009).
- [14] H. Yamamoto, “Resonant tunneling condition and transmission coefficient in a symmetrical one-dimensional rectangular double-barrier system,” *Appl. Phys. A* **42**, 245–248 (1987).
- [15] B. Ricco, M. Ya. Azbel, “Physics of resonant tunneling: The one-dimensional double barrier case,” *Phys. Rev. B* **29**, 1970–1981 (1984).
- [16] J. L. Powell and B. Crasemann, *Quantum Mechanics* (Addison-Wesley, Reading, MA, 1965).
- [17] P. C. W. Davies, “Quantum tunneling time,” *Am. J. Phys.* **73**, 23–27 (2005).
- [18] T. Hartman, “Tunneling of a wave packet,” *J. Appl. Phys.* **33**, 3427–3433 (1962).
- [19] E. H. Hauge and J. A. Stoveng, “Tunneling times: A critical review,” *Rev. Mod. Phys.* **61**, 917–936 (1989)
- [20] V. S. Olkhovsky, E. Recami, and G. Salesi, “Superluminal tunneling through two successive barriers,” *Europhys. Lett.*, **57**, 879–884 (2002).
- [21] V. Petrillo and V. S. Olkhovsky, “Time asymptotic expansion of the tunneled wave function for a double barrier potential,” *Europhys. Lett.* **74**, 327–333 (2006).
- [22] H. G. Winful, “Tunneling time, the Hartman effect and superluminality: A proposed resolution of an old paradox,” *Physics Reports* **436**, 1–69 (2006).
- [23] R. Tsu and L. Esaki, “Tunneling in a finite superlattice,” *Appl. Phys. Lett.* **22**, 562–564 (1973).
- [24] E. Anemogiannis, E. N. Glytsis, and T. K. Gaylord, “Bound and quasibound state calculations for biased/unbiased semiconductor quantum heterostructures,” *IEEE J. Quantum Electronics* **29**, 2731–2740 (1993).
- [25] S. Chand and J. Kumar, “Evidence for the double distribution of barrier heights in Pd<sub>2</sub>Si/n-Si Schottky diodes from I-V-T measurements,” *Semicond. Sci. Technol.* **11**, 1203–1208 (1996).

- [26] S. Zeyrek, M. M. Bulbul, S. Altindal, M. C. Baykul, and H. Yuzer, “The double Gaussian distribution of inhomogeneous barrier heights in Al/GaN/p-GaAs (MIS) Schottky diodes in wide temperature range,” *Braz. J. Phys.* **38**(4), 591–597 (2008).
- [27] L. V. Chebotarev, “Resonant delay in tunnelling through smooth double and triple barriers,” *Phys. Stat. Sol. (b)* **208**, 69–86 (1998).